RESEARCH ARTICLE

Direct Conversion of Hybrid Precoding and Combining From Full Array Architecture to Subarray Architecture for mmWave MIMO Systems

MOHAMED ALOUZI[1], **(Student Member, IEEE), FAISAL AL-KAMALI**[1], **CLAUDE D'AMOURS**[1], **(Member, IEEE), AND FRANCOIS CHAN**[1,2], **(Senior Member, IEEE)**

[1]School of Electrical Engineering and Computer Science, University of Ottawa, Ottawa, ON K1N 6N5, Canada
[2]Department of Electrical and Computer Engineering, Royal Military College, Kingston, ON K7K 7B4, Canada

Corresponding author: Mohamed Alouzi (malou052@uottawa.ca)

ABSTRACT Hybrid precoding and combining for millimeter-wave (mmWave) multiple-input multiple-output (MIMO) systems with subarray (SA) architecture is a promising technology for 6G because of their low complexity, cost, and power consumption compared to the full array (FA) architecture. This paper proposes an iterative algorithm for designing hybrid precoding and combining for the SA architecture. It is called direct conversion of iterative hybrid precoding and combining from FA to SA (DCIFS). The proposed algorithm involves an iterative process that begins by designing a hybrid precoding and combining matrix for the FA structure and then converts it into an SA matrix by setting certain entries to zero while achieving better performance. It does not depend on the antenna array geometry, unlike other techniques such as the orthogonal matching pursuit (OMP) hybrid precoding and combining approach. We investigate the proposed algorithm with two scenarios. In the first scenario, we use the proposed DCIFS scheme only at the base station (BS) and the iterative FA hybrid scheme at the mobile station (MS), whereas in the second, we use the proposed DCIFS scheme at both the BS and the MS. Simulation results demonstrate that the proposed design approach achieves a spectral efficiency comparable to that of the FA hybrid design counterpart, especially for a large system, while maintaining low complexity. For example, when SNR = 0 dB and the number of transmitted streams (N_s) = 2, the proposed algorithm provides about 1.5 bps/Hz spectral efficiency gain compared to the OMP hybrid design for the first scenario. Moreover, when the number of iterations is low and the number of BS antenna and N_s is high, the proposed approach outperforms the conventional SA hybrid design in terms of spectral efficiency with the same hardware complexity.

INDEX TERMS Full array architecture, subarray architecture, hybrid precoding and combining, mmWave MIMO systems.

I. INTRODUCTION

Hybrid precoding is a key technology for massive multiple-input multiple-output (MIMO) systems for millimetre wave (mmWave) communications [1], [2], [3]. The hybrid precoding and combining architectures currently in use can be classified as fully array (FA) [4], [5], [6] or subarray (SA)

The associate editor coordinating the review of this manuscript and approving it for publication was Barbara Masini.

[7], [8]. Numerous papers have been written about the design of hybrid precoding and combining schemes for both narrowband FA [5], [6], [9], [10] and wideband FA [11], [12], [13], [14], [15]. The FA hybrid precoding and combining architecture can provide high spectral efficiency in massive MIMO systems because each RF chain is connected to every antenna via phase shifters [5], [6]. However, this architecture requires a large number of phase shifters, leading to high complexity and power consumption [7], [8]. In [4], it was suggested that

an orthogonal matching pursuit (OMP)-based scheme can be used in light of the mmWave channel's sparse structure. The spectral efficiency optimization problem is modelled in this scheme as a sparse reconstruction issue. In [6], an iterative solution to find a low-complexity hybrid precoding and combining scheme for narrowband mmWave was proposed and studied. In [6], it was shown that the suggested scheme yields a performance that is close the optimal one. Although the FA architecture provides high spectral efficiency, it is complex in massive MIMO systems because each RF chain is connected to all antennas. As a result, the SA architecture is a low complexity alternative for massive MIMO since each RF chain is only connected to a subset of antennas [7], [8].

Recently, SA architectures have received a lot of attention because of their reduced complexity. SA architectures can be categorized into fixed SA [8], [15], [16], [17], [18], [19], [20], [21], [22] and dynamic SA (DSA) [7], [23], and [27]. A closed-form solution for fully connected hybrid precoding based on OFDM is derived in [7] for mmWave systems. This solution is then expanded into DSA. In [8], two low-complexity hybrid precoding algorithms were proposed for the fixed SA architecture mmWave MIMO systems. They divide the hybrid precoding matrix into vectors and determine the analog precoding vector of each subarray from the first vector of the subarray submatrix. Then, to further enhance the system performance, the resulting hybrid precoding is found though an iterative algorithm. A hybrid precoding method based on successive interference cancellation (SIC) was presented and investigated for SA architecture in [16]. Assuming a diagonal digital precoder with real elements, [16] showed that the SA architecture is more energy-efficient than the FA architecture. Two analog precoder methods were proposed by the authors of [18] for situations with high and low signal-to-noise ratios. After selecting the analog precoder, the optimal digital precoder is subsequently produced using a water-filling process. A new hybrid precoding architecture for SA mmWave communication systems was presented in [20]. This architecture uses a two-layer PS network instead of the traditional FC structure to fully utilize the array's beamforming gain with a significantly lower hardware complexity. In [21], a low-complexity hybrid architecture for mmWave multiuser MIMO systems utilizing fixed subarrays and quantized RF phase-shifting networks was developed. Under the assumption that linear zero-forcing was utilized at the digital baseband, the complicated hybrid precoder optimization problem was reduced to an eigenvalue maximization problem. To increase the spectral efficiency of the SA design, the authors of [22] proposed an overlapping SA architecture with iterative hybrid precoding. The results showed that the overlapped SA architecture, while slightly more complex in terms of hardware than the fixed SA architecture, can improve spectral efficiency while still being less complex than the DSA and FA structures.

The hybrid precoding and combining techniques for DSA architecture have been studied in the literature for two scenarios: narrowband [23], [24] and wideband [25], [26], [27], [28]. Although a DSA architecture outperforms a fixed SA architecture in terms of performance, it uses more power than a fixed SA design and has greater hardware and computational complexity. This is because the number of switches necessary increases linearly with the number of transmit antennas. Using a partially dynamic SA structure can reduce the complexity compared to a DSA approach [29], [30]. Researchers in [31] and [32] proposed and studied hybrid precoding designs for adaptive SA structures in mmWave MIMO systems. Different from the aforementioned works that design hybrid precoders and combiners independently, [33] proposed an efficient scheme to jointly design precoding and combining for hybrid beamforming systems with SA architecture.

Deep learning methods have recently been proposed to create hybrid precoding and combining for massive MIMO [34], [35], [36], [37]. In order to improve performance and provide quicker calculation times compared to conventional approaches, a deep learning framework was presented in [34]. In [34], a convolutional neural network for MIMO uses an imperfect channel matrix as an input to produce an analog precoder and combiner as its output. In [36], the authors proposed the unsupervised learning approach to design the hybrid beamforming for SA and showed through simulation that the proposed unsupervised deep learning techniques outperform the conventional hybrid beamforming techniques. In the presence of beam squint, a deep learning-based wideband hybrid precoding network was developed in [37] for Terahertz massive MIMO system.

Previous research in hybrid precoding and combining primarily focused on designing hybrid precoding and combining for either FA or SA structures. However, to the best of our knowledge, no previous work has explored the use of hybrid precoding and combining for FA as a starting point to design that for SA. This paper aims to fill this gap by designing hybrid precoding and combining for fixed SA architectures, based on the hybrid precoder and combiner design of the FA architecture. This new approach can achieve the spectral efficiency of FA architecture while maintaining the same hardware complexity as that of the conventional SA architecture. The main difference between the design method proposed in this paper and that in other papers is the approach taken to design the hybrid precoding and combining matrices of the SA architecture. In other papers, the hybrid precoding and combining matrices are designed separately for each subarray [8]. This approach is known as subarray-wise design, and it involves designing a hybrid precoding and combining matrix for each subarray independently. In contrast, this paper proposes an iterative design approach that uses a FA hybrid precoding and combining matrix to obtain a SA matrix at each iteration. The proposed approach involves first finding the FA hybrid precoding and combining matrix at each iteration and then obtaining a SA matrix by setting certain entries to zero while retaining the same level of performance. The process is

repeated iteratively until the desired performance is achieved. The conventional SA solves all subarray suboptimization problems independently to determine the hybrid precoding and combining of the whole SA architecture, whereas the approach proposed in this paper only solves the optimization problem of the hybrid precoding and combining in the FA architecture and then transforms the resulting FA hybrid precoder and combiner directly to obtain that of the whole SA architecture.

It should be noted that the proposed scheme has the same hardware complexity as the traditional SA and is built for a fixed SA architecture. The design approach and computational complexity are different, as section IV demonstrates. Due to its design for a fixed SA architecture and lack of switch requirements, the suggested method is less expensive, consumes less power, and has lower hardware and computational complexity than the DSA.

The main contributions of this work are summarized as follows:

- This paper proposes an iterative hybrid precoding and combining for SA architecture. It is called direct conversion of iterative hybrid precoding and combining from FA to SA (DCIFS). It finds the hybrid precoding and combining matrix of FA architecture iteratively, and then using it to find SA matrix at each iteration as illustrated in section III.
- The proposed DCIFS algorithm was evaluated by simulations for two scenarios. Simulation results show that the proposed algorithm achieves significant gain compared to the existing SA and FA, especially for a large system, with lower complexity.

The remainder of the paper is organized as follows. The mmWave system model and the problem formulation are discussed in Section II. The proposed DCIFS hybrid precoding is derived and discussed in Section III. In Section IV, the complexity is analyzed. The simulation results are presented in Section V, and conclusions are drawn in Section VI.

We use the following notation throughout this paper: $\mathbb{C}$ represents the set of complex numbers; $\mathbf{A}$ is a matrix; a is a vector; a is a scalar; The conjugate transpose of $\mathbf{A}$ are represented by $\mathbf{A}^H$; $\mathbf{A}_i$ is the ith column of $\mathbf{A}$; $\mathbf{A}_{i,j}$ is the entry on the ith row and j^{th} column of $\mathbf{A}$; $\|\mathbf{A}\|_F$ is the Frobenius norm of $\mathbf{A}$; tr($\mathbf{A}$) is the trace of $\mathbf{A}$; diag($\mathbf{A}$) is a vector formed by the diagonal elements of $\mathbf{A}$; $\oslash$ stands for element-wise division;. $\odot$ is the element-wise multiplication; $\mathbf{I_N}$ is the $N \times N$ identity matrix.

II. SYSTEM MODELS AND PROBLEM FORMULATION

Consider a single user mmWave hybrid precoding system, in which a base station equipped with N_t antennas and N_{tRF} RF chains serve a single mobile station with N_r antennas and N_{rRF} RF chains. The base station transmits N_s independent data streams. In this section we develop the mathematical framework of the FA, the conventional SA, and the proposed SA system models. Figure 1 shows the block diagram of hybrid precoding in the SA architecture.
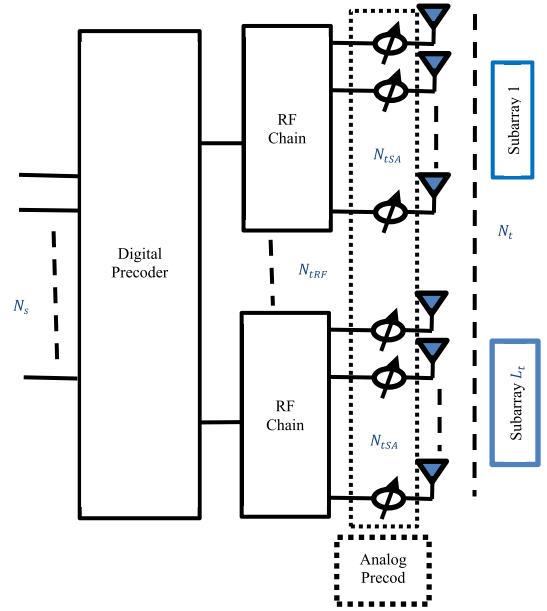

FIGURE 1. Hybrid precoding at the BS for the SA architecture.

A. FA SYSTEM MODEL

In this subsection, a system model of the FA architecture is discussed. The baseband digital precoder $\mathbf{P_D}$ is applied at the transmitter first, and the resulting signal is then precoded by the FA analog precoder $\mathbf{P_{AFA}}$. At the receiver side, the FA analog combiner $\mathbf{W_{AFA}}$ and the digital combiner $\mathbf{W_D}$ are applied. In the FA architecture, the received signal can be written as [6]

$$\begin{aligned} y &= \sqrt{\rho}\mathbf{W_D}^H\mathbf{W_{AFA}}^H\mathbf{H}\mathbf{P_{AFA}}\mathbf{P_D}s + n \\ &= \sqrt{\rho}\mathbf{W_{FA}}^H\mathbf{H}\mathbf{P_{FA}}s + n \end{aligned} \tag{1}$$

where ρ is the average power of the received signal, $\mathbf{H} \in \mathbb{C}^{N_r \times N_t}$ is the channel matrix, $\mathbf{P_{AFA}}$ and $\mathbf{P_D}$ are the $N_t \times N_{tRF}$ and the $N_{tRF} \times N_s$ matrices that represent the FA analog and digital precoding matrices, respectively. $\mathbf{W_{AFA}}$ and $\mathbf{W_D}$ are the $N_r \times N_{rRF}$ and the $N_{rRF} \times N_s$ matrices that represent the FA analog and digital combiner matrices, respectively. The vector s is the $N_s \times 1$ vector that represents the transmitted signal such that $\mathbb{E}\left[ss^*\right] = \frac{1}{N_s}\mathbf{I}_{N_s}$ and n is the $N_s \times 1$ vector of independent and identical distribution $\mathcal{CN}\left(0, \sigma_n^2\right)$ additive white Gaussian noise. $\mathbf{P_{FA}} = \mathbf{P_{AFA}}\mathbf{P_D}$ and $\mathbf{W_{FA}} = \mathbf{W_{AFA}}\mathbf{W_D}$. All elements in $\mathbf{P_{AFA}}$ and $\mathbf{W_{AFA}}$ have the same amplitude, which is equal to $1/\sqrt{N_t}$ and $1/\sqrt{N_r}$, respectively [6]. Additionally, the digital precoder and combiner are also normalized to satisfy the total power constraint, i.e., $\|\mathbf{P_{AFA}}\mathbf{P_D}\|_F^2 = N_s$ and $\|\mathbf{W_{AFA}}\mathbf{W_D}\|_F^2 = N_s$.

In this paper, a mmWave channel model is assumed and the commonly used Saleh-Velenzuela model is used to simulate the channel parameter in outdoor scenarios [6]. Therefore, this paper uses the narrowband clustered channel described in [4], [6], and [8] and $\mathbf{H}$ can be written as

$$\begin{aligned} \mathbf{H} = \sqrt{N_t N_r / N_{cl} N_{ray}} \times \sum_i^{N_{cl}} \sum_l^{N_{ray}} [\alpha_{il} \Gamma_r \left(\phi_{il}^r, \theta_{il}^r\right) \\ \times \Gamma_t \left(\phi_{il}^t, \theta_{il}^t\right) \mathrm{a}_r \left(\phi_{il}^r, \theta_{il}^r\right) \mathrm{a}_t \left(\phi_{il}^t, \theta_{il}^t\right)^*] \end{aligned} \tag{2}$$

where N_{cl} is the number of clusters and N_{ray} is the number of paths. $\alpha_{il} \in \mathbb{C}$ is the gain of the lth path in the ith cluster. $\phi_{il}^t(\phi_{il}^r)$ and $\theta_{il}^t(\theta_{il}^r)$ are the azimuth (elevation) angles of departure and arrival (AODs/AOAs) of the lth path in the ith cluster. $\Gamma_t\left(\phi_{il}^t, \theta_{il}^t\right)$ and $\Gamma_r\left(\phi_{il}^r, \theta_{il}^r\right)$ represent the transmit and receive antenna element gain at their departure and arrival angles. $a_t\left(\phi_{il}^t, \theta_{il}^t\right)$ is the antenna array response at the transmitter and $a_r\left(\phi_{il}^r, \theta_{il}^r\right)$ is the antenna array response at the receiver. The array response vector in a uniform planer array (UPA) is defined as [6]

$$a_{UPA(\phi,\theta)} = \frac{1}{\sqrt{N_t}}[1, \ldots, e^{jkd(xsin(\phi)sin(\theta)+ycos(\theta))},$$
$$\ldots, e^{jkd((w-1)sin(\phi)sin(\theta)+(h-1)cos(\theta))}]^T \quad (3)$$

where $1 \leq x \leq (w-1)$ and $1 \leq y \leq (h-1)$. $d = \lambda/2$, w and h are the inter-antenna spacing, the width and the height of the antenna array, respectively. The array size of the transmitter is $N_t = wh$. In this paper, we assume perfect channel state information at the BS and the MS. The spectral efficiency of the FA architecture can be written as [6]

$$R = \log_2\left(\left|I_{N_r} + \frac{\rho}{N_s}Q_k^{-1}W_B^{k\,H}W_{AFA}^{k\,H}HF_{AFA}\right.\right.$$
$$\left.\left.\times F_B P_B^H P_{AFA}^H H_k^H W_{AFA}^k W_B^k\right|\right) \quad (4)$$

where $Q_k = \sigma_n^2 W_B^{k\,H}W_A^{k\,H}W_A^k W_B^k$. To maximize the spectral efficiency in (4), the total transmitted power constraint as well as the constraint on F_{AFA} and W_{AFA}, should be taken into consideration in the hybrid precoder/combiner design.

$$\max_{P_{AFA},P_D,W_{AFA},W_D} R$$
$$\text{st. } P_{AFA} \mathcal{E} \mathcal{F}_{AFA} \quad \text{and} \quad W_{AFA} \mathcal{E} \mathfrak{I}_{AFA}$$
$$\|P_{AFA}P_D\|_F^2 = N_s \quad (5)$$

where $\mathcal{F}_{AFA}$ and $\mathfrak{I}_{AFA}$ include all possible precoding and combining matrices, respectively, that satisfy the amplitude constraint. Maximizing the objective function in (5) can be expressed more simply as [6]

$$\left(P_{AFA}^{opt}, P_D^{opt}\right) = \arg\min_{P_{AFA},P_D} \left\|P_{FA}^{opt} - P_{AFA}P_D\right\|_F^2$$
$$\text{st. } P_{AFA} \mathcal{E} \mathcal{F}_{AFA},$$
$$\|P_{AFA}P_D\|_F^2 = N_s \quad (6)$$

and

$$\left(W_{AFA}^{opt}, W_D^{opt}\right) = \arg\min_{W_{AFA},W_D} \left\|W_{FA}^{opt} - W_{AFA}W_D\right\|_F^2$$
$$\text{st. } W_{AFA} \mathcal{E} \mathfrak{I}_{AFA},$$
$$\|W_{AFA}W_D\|_F^2 = N_s \quad (7)$$

The problems (6) and (7) are clearly non-convex optimization problems with a difficult optimal solution. The solution of the optimal unconstrained digital precoding is given by $P_{FA}^{opt} = V_1$, where V_1 is the first N_s column of V that is obtained from the singular value decomposition (SVD) of H,

i.e., $H = U\Sigma V^H$. $W_{FA}^{opt} = U_1$, where U_1 represents the first N_s column of U, is the optimal unconstrained solution of the digital combiner.

B. CONVENTIONAL SA SYSTEM MODEL
In this subsection, a system model of the SA architecture is described and the received signal of the SA can be written as

$$y = \sqrt{\rho}W_D^H W_{ACSA}^H HP_{ACSA}P_D s + n \quad (8)$$

where P_{ACSA} is the analog precoding matrix and W_{ACSA} is the analog combining matrix of the conventional SA architecture. Also, P_D is the digital precoding matrix and W_D is the digital combining matrix of the SA architecture For SA architecture, P_{ACSA} and W_{ACSA} can be expressed as

$$P_{ACSA} = \begin{bmatrix} p_{A1} & 0_{N_{tSA}\times 1} & \cdots & 0_{N_{tSA}\times 1} \\ 0_{N_{tSA}\times 1} & p_{A2} & \cdots & \vdots \\ \vdots & \vdots & \ddots & 0_{N_{tSA}\times 1} \\ 0_{N_{tSA}\times 1} & \cdots & 0_{N_{tSA}\times 1} & p_{AN_{tRF}} \end{bmatrix} \quad (9)$$

and

$$W_{ACSA} = \begin{bmatrix} w_{A1} & 0_{N_{rSA}\times 1} & \cdots & 0_{N_{rSA}\times 1} \\ 0_{N_{rSA}\times 1} & w_{A2} & \cdots & \vdots \\ \vdots & \vdots & \ddots & 0_{N_{rSA}\times 1} \\ 0_{N_{rSA}\times 1} & \cdots & 0_{N_{rSA}\times 1} & w_{AN_{rRF}} \end{bmatrix} \quad (10)$$

where p_{Al} is the $N_{tSA} \times 1$ analog precoding vector of the lth subarray ($l = 1, 2, \ldots, N_{tRF}$) whose elements have the same amplitude $1/\sqrt{N}_{tSA}$ but different phases. w_{Al} represents the $N_{rSA} \times 1$ analog combining vector of the of the lth subarray ($l = 1, 2, \ldots, N_{rRF}$) whose elements have the same amplitude $1/\sqrt{N}_{rSA}$ but different phases. $N_{tSA} = N_t/N_{tRF}$ and $N_{rSA} = N_r/N_{rRF}$ are the number of elements in each SA at the transmitter and at the receiver, respectively.

The optimization problem of the lth subarray can be written as [8]

$$\left(p_{Al}^{opt}, p_{Dl}^{opt}\right) = \arg\min_{p_{Al},p_{Dl}} \left\|P_l^{opt} - p_{Al}p_{Dl}\right\|_F^2$$
$$\text{st. } p_{Al} \mathcal{E} \overline{\mathcal{F}}_A,$$
$$\|P_{ACSA}P_D\|_F^2 = N_s \quad (11)$$

where $P_l^{opt} = V_1((l-1)N_{tSA} + 1 : lN_{tSA}, :)$ is the optimum unconstrained digital precoding solution of the lth subarray. p_{Dl} is the lth row of the P_D. $\overline{\mathcal{F}}_A$ includes all possible $N_{tSA} \times 1$ vectors satisfying the amplitude constraint. The solution of this problem was discussed in detail in [8].

C. PROPOSED SA SYSTEM MODEL
In this subsection, the proposed SA system model for the SA architecture is studied. It aims to convert the FA system model into SA system model. At the receiver side, the received signal can be given as

$$y = \sqrt{\rho}W_D^H W_{APSA}^H HP_{APSA}P_D s + n \quad (12)$$

where $\mathbf{P_{APSA}}$ and $\mathbf{W_{APSA}}$ are the analog precoding and combining matrices of the proposed SA system model. In the proposed SA model, $\mathbf{P_{APSA}}$ and $\mathbf{W_{APSA}}$ can be expressed as

$$\mathbf{P_{APSA}} = \mathbf{P_{AFA}} \odot \mathbf{T_P}, \quad \text{and} \quad \mathbf{W_{APSA}} = \mathbf{W_{AFA}} \odot \mathbf{T_W} \tag{13}$$

where $\mathbf{T_P}$ and $\mathbf{T_W}$ are the transformation matrices that are used to transform the analog precoding and combining matrices of FA into SA matrices and their dimensions are the same as those of the $\mathbf{P_{AFA}}$ and $\mathbf{W_{AFA}}$. $\odot$ is the element-wise multiplication. $\mathbf{T_P}$ and $\mathbf{T_W}$ can be given as

$$\mathbf{T_P} = \begin{bmatrix} 1_{N_{tSA} \times 1} & 0_{N_{tSA} \times 1} & \cdots & 0_{N_{tSA} \times 1} \\ 0_{N_{tSA} \times 1} & 1_{N_{tSA} \times 1} & \cdots & \vdots \\ \vdots & \vdots & \ddots & 0_{N_{tSA} \times 1} \\ 0_{N_{tSA} \times 1} & \cdots & 0_{N_{tSA} \times 1} & 1_{N_{tSA} \times 1} \end{bmatrix} \tag{14}$$

and

$$\mathbf{T_W} = \begin{bmatrix} 1_{N_{rSA} \times 1} & 0_{N_{rSA} \times 1} & \cdots & 0_{N_{rSA} \times 1} \\ 0_{N_{rSA} \times 1} & 1_{N_{rSA} \times 1} & \cdots & \vdots \\ \vdots & \vdots & \ddots & 0_{N_{rSA} \times 1} \\ 0_{N_{rSA} \times 1} & \cdots & 0_{N_{rSA} \times 11} & 1_{N_{rSA} \times 1} \end{bmatrix} \tag{15}$$

where $1_{N_{rSA} \times 1}$ and $0_{N_{rSA} \times 1}$ are $N_{rSA} \times 1$ vectors of ones and zeros, respectively. The problem formulation of the hybrid precoding and combining in the proposed SA system model will be discussed and solved in the next section.

III. PROPOSED DCIFS HYBRID PRECODING AND COMBINING ALGORITHM

In this section, we propose the low complexity DCIFS hybrid precoding and combining algorithm and derive the equations that relate to the precoder only since the derivation of the combiner is similar. We note that the optimal unconstrained semi-unitary precoder for $\mathbf{H}$ is simply given by $\mathbf{P_{FA}^{opt}} = \mathbf{V_1}$, where $\mathbf{V_1^H V_1} = \mathbf{I_{N_s}}$. Also, we need the hybrid precoder $\mathbf{P_{APSA} P_D}$ to be sufficiently "close" to the optimal precoder $\mathbf{V_1}$ by using its digital precoder to construct linear combinations of the RF precoder vectors. Since $\mathbf{P_{APSA}}$ is a semi-diagonal matrix, this matrix is totally non-square semi-unitary after its element-wise normalization, i.e., $\mathbf{P_{APSA}^H P_{APSA}} = \mathbf{I_{N_{tRF}}}$. In addition, the digital precoding $\mathbf{P_D}$ can be totally unitary $\mathbf{P_D^H P_D} = \mathbf{P_D P_D^H} = \mathbf{I_{N_S}}$ or a non-square matrix that is totally semi-unitary $\mathbf{P_D^H P_D} = \mathbf{I_{N_S}}$. This structure will be reflected when solving the optimization problem to make the hybrid precoder $\mathbf{P_{APSA} P_D}$ sufficiently "close" to the optimal precoder $\mathbf{V_1}$ since the optimal unconstrained precoder $\mathbf{V_1}$ is semi-unitary matrix. Thus, by knowing this information about hybrid precoder $\mathbf{P_{APSA} P_D}$, we

need to solve the following optimization problem

$$\left(\mathbf{P_{APSA}^{opt}}, \mathbf{P_D^{opt}}\right) = \underset{\mathbf{P_{APSA}}, \mathbf{P_D}}{\arg min} \left\| \mathbf{P_{FA}^{opt}} - \mathbf{P_{APSA} P_D} \right\|_F^2$$
$$st. \ \mathbf{P_{APSA}} \, \mathcal{E} \, \mathbf{F_{AFA}},$$
$$\mathbf{P_{APSA}^H P_{APSA}} = \mathbf{I_{N_{tRF}}} \text{ and } \mathbf{P_D^H P_D} = \mathbf{I_{N_s}}$$
$$\left\| \mathbf{P_{APSA} P_D} \right\|_F^2 = N_s \tag{16}$$

The problem (16) is non-convex optimization problem with a difficult optimal solution. However, by knowing that the structure of $\mathbf{P_{APSA}}$ is totally non-square semi-unitary and assuming $\mathbf{P_D}$ is totally unitary or semi-unitary matrix, the iterative solution to (16) can be obtained by solving the following optimization problem

$$\left(\mathbf{P_{APSA}^{opt}}, \mathbf{P_D^{opt}}\right) = \underset{\mathbf{P_{APSA}}, \mathbf{P_D}}{\arg min} \left\| \mathbf{P_{FA}^{opt}} - \mathbf{P_{APSA} P_D} \right\|_F^2 \tag{17}$$

We first need to find the baseband precoder $\mathbf{P_D}$ that minimizes the Euclidean distance by using the initialization of the proposed RF precoder $\mathbf{P_{APSA}}$, which is calculated by taking the first N_{tRF} columns from $\mathbf{P_{FA}^{opt}}$ and then normalizing them such that each entry has constant magnitude, i.e., $\mathbf{P_{APSA}} = (\mathbf{P_{FA}^{opt}} \oslash (|\mathbf{P_{FA}^{opt}}| \sqrt{N_{tSA}})) \odot \mathbf{T_P}$. One should note that the element-wise normalization of $\mathbf{P_{APSA}}$ satisfies the normalization constraint $|[\mathbf{P_{APSA}}]_{i,j}|^2 = 1/N_{tSA}$. We then find the RF precoder $\mathbf{P_{APSA}}$ such that the hybrid precoder $\mathbf{P_{APSA} P_D}$ is sufficiently "close" to the optimal unconstrained digital precoder $\mathbf{V_1}$. Specifically, we would like to solve the following alternating optimization problem first, which is related to (17):

$$\left(\mathbf{P_D^{opt}}\right) = \underset{\mathbf{F_D}}{\arg \min} \left\| \mathbf{P_{FA}^{opt}} - \mathbf{P_{APSA} P_D} \right\|_F^2 \tag{18}$$

The objective function can be expanded as

$$\left\| \mathbf{P_{FA}^{opt}} - \mathbf{P_{APSA} P_D} \right\|_F^2$$
$$= \text{tr}\left(\mathbf{P_{FA}^{opt H} P_{FA}^{opt}}\right) - 2\text{tr}\left(\mathbf{P_{FA}^{opt H} P_{APSA} P_D}\right) + \left\| \mathbf{P_{APSA} P_D} \right\|_F^2$$
$$= 2N_S - 2\text{tr}\left(\mathbf{P_{FA}^{opt H} P_{APSA} P_D}\right) \tag{19}$$

The solution of this problem, which is to find the maximization of $\mathbf{P_{FA}^{opt H} P_{APSA} P_D}$ is solved by what is called the orthonormal Procrustes problem [38] as

$$\mathbf{P_D} = \mathbf{V U^H} \tag{20}$$

where $\mathbf{P_{FA}^{opt H} P_{APSA}} = \mathbf{U \Sigma V^H}$. Then, we keep $\mathbf{P_D}$ fixed and solve the same optimization problem but now minimizing over $\mathbf{P_{APSA}}$ as follows [39]:

$$\left(\mathbf{P_{APSA}^{opt}}\right) = \underset{\mathbf{P_{AFS}}}{\arg \min} \left\| \mathbf{P_{FA}^{opt}} - \mathbf{P_{APSA} P_D} \right\|_F^2 \tag{21}$$

Similar to (19), expanding the objective function yields

$$\left\| \mathbf{P_{FA}^{opt}} - \mathbf{P_{APSA} P_D} \right\|_F^2 = 2N_S - 2\text{tr}\left(\mathbf{P_{FA}^{opt H} P_{APSA} P_D}\right) \tag{22}$$

Given that, the optimal unconstrained matrix $\mathbf{V_1}$ is totally semi-unitary and the digital precoding $\mathbf{P_D}$ is totally unitary or semi-unitary non-square matrix, the solution that maximize $\mathbf{P_{FA}^{opt}}^H \mathbf{P_{APSA}} \mathbf{P_D}$ in (22) is given as follows

$$\mathbf{P_{APSA}} = \mathbf{P_{FA}^{opt}} \mathbf{P_D}^H \qquad (23)$$

The main difference between the hybrid design in this paper and that in [39] is that our design is more general and can work in all scenarios whether the number of data streams equals the number of RF chains or the number of data streams is less than the number of RF chains. However, HD-AM can only work when the number of data streams equals the number of RF chains. Furthermore, our derivation is based on the SA architecture and thanks to the structure of $\mathbf{P_{APSA}}$, which is totally non-square semi-unitary matrix. HD-AM, on the other hand, is derived only for the FA architecture.

The pseudo-code for the proposed DCIFS hybrid precoder $\mathbf{P_{APSA}}$ solution is given in Algorithm 1. The inputs of the algorithm are $\mathbf{P_{FA}^{opt}} \in C^{N_t \times N_S}$, initialized analog procoder $\mathbf{P_{APSA}} \in C^{N_t \times N_{tRF}}$ i.e., $\mathbf{P_{APSA}} = \left(\mathbf{P_{FA}^{opt}} \oslash \left(\left| \mathbf{P_{FA}^{opt}} \right| \sqrt{N_{tSA}} \right) \right) \odot \mathbf{T_P}$, and the maximum number of iterations K, where $K \geq 1$ for $N_S < N_{tRF}$ or $N_{tRF} = N_S$. In the general case of $N_S \geq 1$ where $N_S \leq N_{tRF}$, the algorithm starts by computing $\mathbf{P_D}$ using the orthonormal Procrustes solution in step 2. After that, the algorithm proceeds to update the proposed RF precoder $\mathbf{P_{APSA}}$ in steps 3. Step 4 ensures that the proposed RF precoder $\mathbf{P_{APSA}}$ is satisfied exactly with constant-magnitude entries which can be applied at RF using analog phase shifters. In step 5, we make sure that $\mathbf{P_{APSA}}$ still has the subarray structure. After the last iteration of the algorithm, $\mathbf{P_D}$ is updated via the maximal ratio combining (MRC) instead of the least squares solution which has an impact on Frobenius norm objective function [4]. Based on our results, step 7 reduces the Frobenius norm objective function $\left\| \mathbf{P_{FA}^{opt}} - \mathbf{P_{APSA}} \mathbf{P_D} \right\|_F$ because the least squares solution becomes MRC after implementing the semi-unitary proposed analog precoder, i.e., $\mathbf{P_{APSA}^H} \mathbf{P_{APSA}} = \mathbf{I_{N_{tRF}}}$. After K iterations the process is completed and the algorithm finds the $N_t \times N_{tRF}$ proposed RF precoding matrix $\mathbf{P_{APSA}}$ and the proposed $N_{tRF} \times N_S$ baseband precoder $\mathbf{P_D}$ such that $\left\| \mathbf{P_{FA}^{opt}} - \mathbf{P_{APSA}} \mathbf{P_D} \right\|_F$ is minimized. In steps 8 and 9, we ensure that the transmit power constraint is satisfied and return the proposed hybrid precoder $\mathbf{P_{PSA}} = \mathbf{P_{APSA}} \mathbf{P_D}$. The proposed DCIFS hybrid combiner $\mathbf{W_{PSA}}$ can be calculated in the same way.

IV. COMPLEXITY ANALYSIS OF THE PROPOSED ALGORITHM
In this section, we analyze the complexity in implementing the proposed DCIFS hybrid precoding and combining design using Algorithm 1. To simplify the complexity analysis, let us denote $N = \max\{N_t, N_r\}$, $N_{RF} = \max\{N_{tRF}, N_{rRF}\}$, $N_{SA} = \max\{N_{tSA}, N_{rSA}\}$ and K is the maximum number of iterations of the proposed hybrid design, HD-AM design, and

---

Algorithm 1 Proposed DCIFS Hybrid Precoding

Input: The optimum unconstrained solution $\mathbf{P_{FA}^{opt}} \in C^{N_t \times N_S}$, initialized analog procoder $\mathbf{P_{APSA}} \in C^{N_t \times N_{tRF}}$ with the element-wise normalization, and the maximum number of iterations K.

Output: Analog $\mathbf{P_{APSA}} \in C^{N_t \times N_{tRF}}$ with the element-wise normalization and baseband $\mathbf{P_D} \in C^{N_{tRF} \times N_S}$ such that $\|\mathbf{P_{FA}^{opt}} - \mathbf{P_{PSA}}\|_F$ is reduced and $\|\mathbf{P_{PSA}}\|_F^2 = N_S$, where $\mathbf{P_{PSA}} = \mathbf{P_{APSA}} \mathbf{P_D}$.

1: **for** $i = 1 : K$ **do**
2:    Update: $\mathbf{P_D} = \mathbf{VU^H}$, where $\mathbf{P_{FA}^{opt}}^H \mathbf{P_{APSA}} = \mathbf{U\Sigma V^H}$
3:    Update: $\mathbf{P_{AFA}} = \mathbf{P_{FA}^{opt}} \mathbf{P_D}^H$
4:    Element-Wise Normalization: $\mathbf{P_{APSA}} = \mathbf{P_{AFA}} \oslash (|\mathbf{P_{AFA}}| \sqrt{N_{tSA}})$
5:    $\mathbf{P_{APSA}} = \mathbf{P_{AFA}} \odot \mathbf{T_P}$
6: **end for**
7: $\mathbf{P_D} = \mathbf{P_{APSA}^H} \mathbf{P_{FA}^{opt}}$
8: $\mathbf{P_D} = \sqrt{N_S} \frac{\mathbf{P_D}}{\|\mathbf{P_{APSA}} \mathbf{P_D}\|_F}$
9: Return $\mathbf{P_{PSA}} = \mathbf{P_{APSA}} \mathbf{P_D}$.

TABLE 1. Complexity of the proposed algorithm compared to previous methods from the literature.

Method	Constraints	Phase Shifters Number	Complexity
Sparse Hybrid Design [4]	RF precoding/Combining codebooks	NN_{RF}	$O(N^2 N_{RF} N_S)$
HD-AM Hybrid Design [29]	$N_S = N_{RF}$	NN_{RF}	$O(NN_S^2 K)$
IFA Hybrid Design [6]	None	NN_{RF}	$O(NN_{RF}^2 K)$
SA Hybrid Design [8]	None	N	$O(N_{SA} N_{RF} N_S K)$
Proposed DCIFS Hybrid Design	None	N	$O(NN_{RF} N_S K)$

SA hybrid design. In this section, we present the complexity analysis by evaluating the total number of floating-point operations per second (flops) for each hybrid precoding and combining approach.

The primary factor in the sparse hybrid precoder and combiner design algorithm's complexity depends on the squared maximum number of antennas. The complexity increases nonlinearly when the maximum number of antennas increases. Thus, as we can see in Table 1, the complexities of the proposed DCIFS hybrid design, SA hybrid design [8], IFA hybrid design [6], and HD-AM hybrid design [29] are very low compared to that of the sparse hybrid precoding [4], which requires $O(N^2 N_{RF} N_S)$. Also, the computational complexities of the proposed DCIFS hybrid design, SA hybrid design [8], IFA Hybrid Design, and HD-AM are almost the same, especially when $N \gg N_S$. In terms of hardware complexity, the proposed DCIFS hybrid design, and the SA hybrid design require lower hardware cost compared to the sparse

hybrid design, IFA hybrid design, and HD-AM hybrid design; the number of required phase shifters with the proposed DCIFS hybrid design, and SA hybrid design is N, whereas the other methods require NN_{RF}. Thus, we conclude that the proposed DCIFS hybrid design has lower computational and hardware complexities than the FA hybrid design.

V. SIMULATION RESULTS

This section presents the numerical results to show the performance advantages of the proposed hybrid precoding and combining implemented as described in Algorithm 1. Specifically, we show numerical simulations of the proposed methods' performance when maximizing the spectral efficiency as defined in (4).

In these simulations, we use the system architecture presented in Fig. 1. We consider the case where there is only one BS and one MS at a distance of 100 meters. The spacing between antenna elements is equal to $\lambda/2$. The system is assumed to operate at a 28 GHz carrier frequency in an outdoor scenario, and with a path loss exponent $n = 3.4$. The channel model is described in (2), with $\overline{P_{\alpha,1}} = 1$ for all clusters. The azimuth and elevation angles AoAs/AoDs of the rays within a cluster are assumed to be randomly Laplacian distributed. The AoAs/AoDs azimuths and elevations of the cluster means are assumed to be uniformly distributed. We use the AoD/AoA beamforming codebooks (exact array response of mmWave channel) at the BSs and MSs, respectively for the sparse hybrid design. The *SNR* in all the plots is defined as $SNR = \rho/\sigma^2$. We assume perfect CSI at the BS and MS. For fairness, the same total power constraint is enforced on all precoding/combining solutions.

We divide our results into two scenarios. The first scenario presents the results of implementing the DCIFS hybrid precoding design using Algorithm 1 at the BS, and IFA hybrid combining design [6] at the MS. Then, the second scenario shows the results by using the DCIFS hybrid precoding and combining design at both the BS and the MS. For a fair comparison, we do the same thing for the subarray iterative hybrid design [8]. For both scenarios, we compare the proposed DCIFS hybrid design with the FA sparse hybrid design [4], IFA hybrid design [6], optimal unconstrained digital method, and the SA hybrid design [8].

A. DCIFS HYBRID PRECODING DESIGN AT THE BS, AND ITERATIVE FA HYBRID COMBINING DESIGN AT THE MS

Fig. 2 shows the spectral efficiency achieved by the proposed hybrid DCIFS design, the FA sparse hybrid design [4], the optimal unconstrained digital design, IFA hybrid design [6], and the SA hybrid design [8] in a 144×64 UPAs mmWave system for different *SNR* values with $N_S \in \{1, 2, 3\}$, and $N_{tRF} = N_{rRF} = 4$. The maximum number of iterations K for the proposed DCIFS hybrid design and the SA hybrid design is equal to 1, and 10 for all data streams N_S. In addition, the maximum number of iterations K for IFA hybrid precoding and combining design is 10 for all data streams and for all cases. The proposed DCIFS hybrid design and the SA hybrid
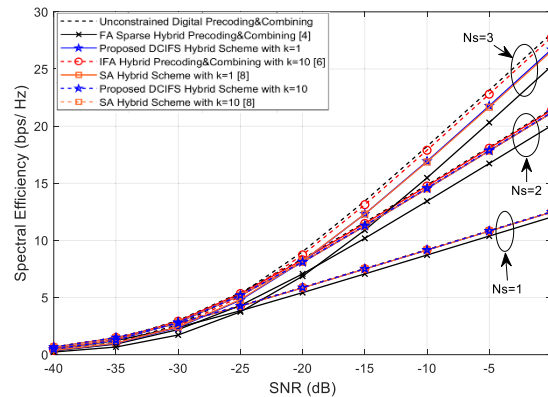

FIGURE 2. Average spectral efficiency achieved by the proposed DCIFS hybrid precoder design with K = 1, and 10 and IFA hybrid combiner with K = 10 compared to the FA sparse hybrid precoders/combiners design [4], the optimal unconstrained digital precoders/combiners, IFA hybrid precoders/combiners design [6], and the SA hybrid precoder design with K = 1, and 10 [8] and IFA hybrid combiner with K = 10 for a 144 × 64 UPAs mmWave systems for different SNR values with $N_S \in \{1, 2, 3\}$, and $N_{tRF} = N_{rRF} = 4$.
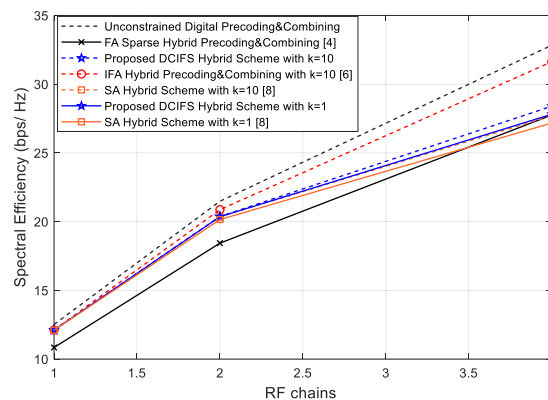

FIGURE 3. Average spectral efficiency achieved by the proposed DCIFS hybrid precoder design with different K and IFA Hybrid Combiner with K = 10 compared to the full array sparse hybrid precoders/combiners [4], the optimal unconstrained digital precoders/combiners, IFA hybrid precoders/combiners [6] with K = 10, and the SA hybrid precoder design with different K and IFA hybrid combiner with K = 10 in 144 × 64 UPAs mmWave systems for SNR = 0 dB with $N_S = N_{tRF} = N_{tRF}$.

design outperform the FA sparse hybrid design, regardless of the number of data streams N_S. The proposed DCIFS hybrid design overlaps the SA hybrid design for any number of data streams with any number of iterations K and both achieve the optimal performance of the unconstrained digital design for $N_S = 1$, and 2. However, when $N_S = 3$, the IFA hybrid design outperforms the proposed DCIFS, and the SA hybrid design.

When the number of RF chains equals the number of data streams, Fig. 3 shows the spectral efficiency achieved by the proposed DCIFS hybrid design with $K = 1$, and 10, the FA sparse hybrid precoders/combiners, the optimal unconstrained digital precoders/combiners, IFA hybrid design with $K = 10$, and the SA hybrid design with $K = 1$ and 10 for different numbers of RF chains and data streams varying from 1 to 4 in a 144×64 UPAs mmWave systems where $N_S = N_{tRF} = N_{rRF}$. The *SNR* is fixed to 0 dB for any number of RF chains. We can see that the proposed DCIFS hybrid design and the SA hybrid design are overlapped when

$N_S = N_{tRF} = N_{rRF} = 1$ and 2; also, they yield an improvement over the FA sparse hybrid design, and both achieve a performance close to that of the IFA hybrid design for any number of iterations. However, when $N_S = N_{tRF} = N_{rRF} = 4$, the overall performance of the proposed DCIFS and SA hybrid design is degraded because of the data streams interference; the proposed DCIFS design with $K = 10$ outperforms the FA sparse hybrid design whereas the SA hybrid design with K = 10 overlaps with the FA sparse hybrid design. The proposed DCIFS hybrid design outperforms the SA hybrid design when the number of RF chains equals to 4 for any number of iterations K.

Fig. 4 evaluates the performance when the number of RF chains is greater than the number of data streams, where $N_S \in \{1, 2, 4\}$ and the *SNR* is fixed to 0 dB over the whole range of RF chains. The proposed DCIFS hybrid design and the SA hybrid design perform better than the FA sparse hybrid method when $N_S = 1$, and 2 for any number of K with small difference between $K = 1$, and $K = 10$. The proposed DCIFS hybrid design with $K = 1$ can accurately approximate the optimal unconstrained one when the number of RF chains is twice the number of data streams when $N_S = 1$, and 2. When $N_S = 4$, the performance of the proposed DCIFS is better than the SA hybrid design for any number of K and the FA sparse hybrid design for $K = 10$; however, both designs have a degradation compared to the FA sparse hybrid design and the optimal unconstrained design when the number RF chains increases because of the high interference between data streams.

Fig. 5 shows the spectral efficiency achieved by the proposed DCIFS hybrid design, the FA sparse hybrid precoding and combining design [4], the optimal unconstrained digital precoding/combining design, IFA hybrid precoding and combining design [6], and the SA hybrid [8] in a UPAs mmWave system for different BS antenna values with $N_r = 64$, $SNR = 0$, $N_S = 2$, and $N_{tRF} = N_{rRF} = 4$. The maximum number of iterations K for the proposed DCIFS hybrid design and the SA hybrid design is equal to 1, and 10 for all number of BS antenna. In addition, the maximum number of iterations K for IFA hybrid precoding and combining design is 10. The performance of the proposed DCIFS and SA hybrid design is better than the FA sparse hybrid design for all cases. However, the IFA hybrid precoding and combining design outperforms the proposed DCIFS and the SA hybrid design for all cases. The performance of the proposed DCIFS hybrid design is better than that of the SA hybrid design for a smaller number of BS antennas and becomes much better for a larger number of BS antennas. The gap between K = 1 and K = 10 for the proposed DCIFS hybrid design is small for any number of BS antennas. However, the gap between K = 1 and K = 10 for the SA hybrid design is bigger especially as the number of BS antennas increases. Thus, using a small number of iterations such as $K = 1$ for the proposed DCIFS hybrid design is enough for any number of BS antennas. The performance of the proposed DCIFS hybrid design with $K = 1$ is the same as that of the SA hybrid design with K = 10, which

means that our design with a very small number of iterations K performs better than the SA design resulting in a reduced computational complexity.
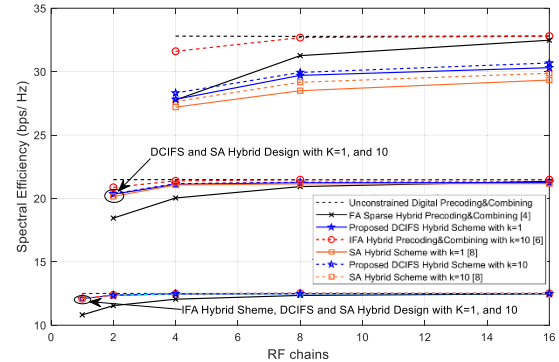

FIGURE 4. Average spectral efficiency achieved by the proposed DCIFS hybrid precoder design with different K and IFA hybrid combiner with K = 10 compared to the FA sparse hybrid precoders/combiners [4], the optimal unconstrained digital precoders/combiners, IFA hybrid precoders/combiners [6] with $K = 10$, and the SA hybrid precoder design with different K and IFA hybrid combiner with K = 10 in 144 × 64 UPAs mmWave systems for SNR = 0 dB with $N_S \in \{1, 2, 4\}$ and different RF chains.
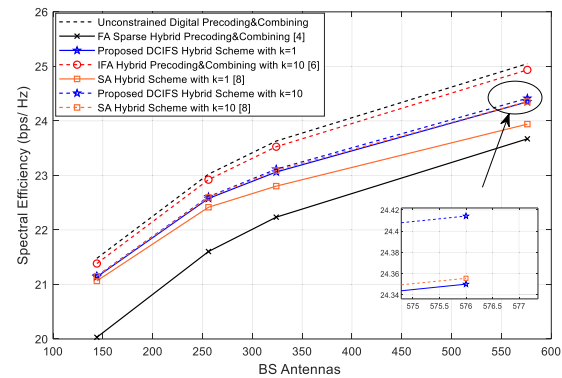

FIGURE 5. Average spectral efficiency vs the number of BS antenna achieved by the proposed DCIFS hybrid precoder design with different K and IFA hybrid combiner with K = 10 compared to the full array sparse hybrid precoders/combiners [4], the optimal unconstrained digital precoders/combiners, IFA hybrid precoders/combiners [6] with $K = 10$, and the SA hybrid precoder design [8] with different K and IFA hybrid combiner with K = 10 in UPAs mmWave systems for $N_r = 64$ with SNR = 0 dB, $N_S = 2$ and $N_{tRF} = N_{rRF} = 4$.

In Fig 6, we utilize the same parameters used in Fig 5, but we increase the number of data streams to 4. As we see in Fig 6, the IFA still outperforms the other designs. The proposed DCIFS hybrid design outperforms the FA sparse hybrid design for $K = 10$ and the gain is small when K = 1. The SA hybrid design performs similarly to the FA sparse design for a small number of BS antennas when K = 10. However, for larger number of BS antennas, the SA hybrid design yields a lower performance for any number of iterations K. The gap between $K = 1$ and $K = 10$ for the proposed DCIFS hybrid design is smaller for any number of BS antennas compared to the gap between $K = 1$ and $K = 10$ for the SA hybrid design, especially for a higher number of BS antennas.

In conclusion, due to the structure of the analog and baseband precoding/combing matrices, the proposed DCIFS hybrid design provides a higher gain compared to the FA
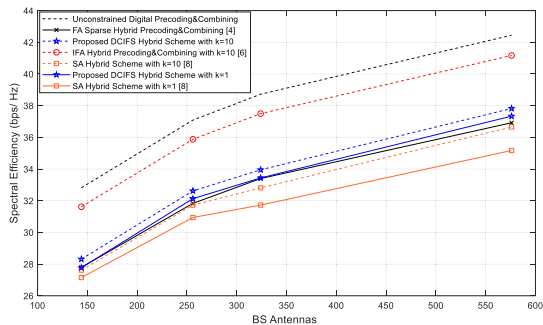
FIGURE 6. Average spectral efficiency vs the number of BS antenna achieved by the proposed DCIFS hybrid precoder design with different K and IFA Hybrid Combiner with K = 10 compared to the full array sparse hybrid precoders/combiners [4], the optimal unconstrained digital precoders/combiners, IFA hybrid precoders/combiners [6] with K = 10, and the SA hybrid precoder design [8] with different K and IFA Hybrid Combiner with K = 10 in UPAs mmWave systems for N_r = 64 with SNR = 0 dB, N_S = 4 and $N_{tRF} = N_{rRF}$ = 4.

sparse hybrid design and the SA hybrid design for any number of data streams, especially for a large number of BS antennas with a small number of iterations. The number of iterations should be 10 or less because the gain after that will be very small which is confirmed by results that we did not include here in this paper. For a large number of RF chains, more than 4, the proposed DCIFS hybrid design performs poorly when compared to all FA methods, which have a smaller data streams interference. However, in practice, the number of RF chains will be limited because of the high-power consumption and cost per RF chain. The IFA hybrid design outperforms the proposed DCIFS hybrid design for all cases, but its hardware complexity is much higher, and the number of phase shifters is higher in the BS side.

B. DCIFS HYBRID PRECODING DESIGN AT THE BS, AND DCIFS HYBRID COMBINING DESIGN AT THE MS

Fig. 7 shows the spectral efficiency achieved by the proposed DCIFS hybrid precoding and combining design, the FA sparse hybrid precoding and combining design [4], the optimal unconstrained digital precoding/combining design, the IFA hybrid precoding and combining design [6], and the SA hybrid precoding and combining design [8] in a 144 × 64 UPAs mmWave system for different *SNR* values with $N_S \in \{1, 2\}$, and $N_{tRF} = N_{rRF} = 4$. The maximum number of iterations K for the proposed DCIFS hybrid precoding and combining design and the SA hybrid precoding and combining design is equal to 1, and 10 for all data streams N_S. In addition, the maximum number of iterations K for IFA hybrid precoding and combining design is 10. The performance of the proposed DCIFS hybrid precoding and combining design and the SA hybrid precoding and combining is close to that of the optimal unconstrained one and overlapped with the FA sparse hybrid design for $N_S = 1$. However, when $N_S = 2$, the proposed DCIFS hybrid precoding and combining design outperforms the SA hybrid precoding and combining and its performance is close to that of the FA sparse hybrid deign when K = 10. The overall performance of the proposed

DCIFS hybrid precoding and combining design and the SA hybrid precoding and combining design is degraded compared to the results in subsection V-A because the subarray design is used in both the transmitter and the receiver.

Similarly to what was done in the previous subsection, we evaluate the performance when the number of RF chains equals the number of data streams. Fig. 8 shows the spectral efficiency achieved by the proposed DCIFS hybrid precoding and combining design with $K = 1$ and 10, the FA sparse hybrid precoders/combiners, the optimal unconstrained digital precoders/combiners, the IFA hybrid precoding and combining design with $K = 10$, and the SA hybrid precoding and combining design with $K = 1$ and 10 for different numbers of RF chains and data streams varying from 1 to 4 in a 144 × 64 UPAs mmWave systems where $N_S = N_{tRF} = N_{rRF}$.
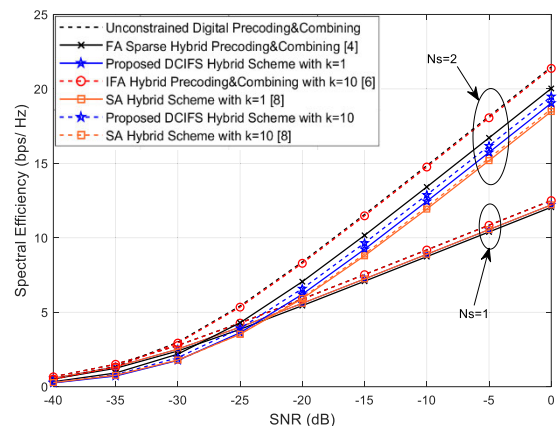

FIGURE 7. Average spectral efficiency achieved by the proposed DCIFS precoders/combiners with K = 1, and 10 compared to the FA sparse hybrid precoding/combining design [4], the optimal unconstrained digital precoders/combiners, the IFA hybrid precoders/combiners [6], and the SA hybrid precoders/combiners [8] for a 144 × 64 UPAs mmWave systems for different SNR values with $N_S \in \{1, 2\}$, and $N_{tRF} = N_{rRF}$ = 4.
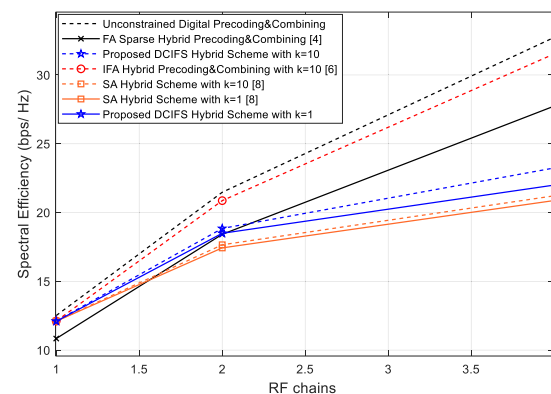

FIGURE 8. Average spectral efficiency achieved by the proposed DCIFS hybrid precoders/combiners with different K compared to the FA sparse hybrid precoders/combiners [4], the optimal unconstrained digital precoders/combiners, IFA hybrid precoders/combiners [6] with K = 10, and the SA hybrid precoders/combiners with different K in 144 × 64 UPAs mmWave systems for SNR = 0 dB with $N_S = N_{tRF} = N_{rRF}$.

The *SNR* is fixed to 0 dB for any number of RF chains. As we can see in Fig 8, the overall performance of the proposed DCIFS and SA hybrid precoding and combining design is worse compared to the results in the previous subsection

in Fig 3; this is because we use the SA architecture in both the transmitter and receiver. The data streams interference increases with the data streams, resulting in an increased gap between the proposed DCIFS and SA hybrid precoding and combining design and the other FA designs. The performance of the proposed DCIFS hybrid precoding and combining design overlaps with the performance of the SA hybrid design when $N_S = 1$. However, for a higher number of data streams, the performance of the DCIFS design is much better than that of the SA design for any number of iterations K.

Fig. 9 evaluates the performance when the number of RF chains is greater than the number of data streams, where $N_S \in \{1, 2, 4\}$ and the SNR is fixed to 0 dB over the whole range of RF chains. Using the SA design in both the transmitter and receiver leads to a degradation in the overall performance of the proposed DCIFS hybrid precoding/combing design and of the SA hybrid precoding/combing design compared to the results in Fig 4; the overall performance becomes worse when the interference between data streams increases for $N_S = 2$ and 4. Similar to Fig. 6, the performance of the proposed DCIFS hybrid precoding and combining design overlaps with the performance of the SA hybrid design for $N_S = 1$ and outperforms the SA design for any number of iterations K for $N_S = 2$ and 4.

Fig. 10 shows the spectral efficiency achieved by the proposed DCIFS hybrid design, the FA sparse hybrid precoding and combining design [4], the optimal unconstrained digital precoding and combining design, the IFA hybrid precoding/combining design [6], and the SA hybrid [8] in a mmWave system for different BS antenna values with $N_r = 64$, $SNR = 0$, $N_S = 2$ and $N_{tRF} = N_{rRF} = 4$. The maximum number of iterations K for the proposed DCIFS hybrid precoding and combining design and the SA hybrid precoding and combining design is equal to 1, and 10 for all BS antennas. In addition, the maximum number of iterations K for IFA hybrid precoding and combining design is 10. The performance of the proposed DCIFS and SA hybrid design is degraded compared to the results in Fig. 5 because we use the SA architecture in BS and MS. The performance of the proposed DCIFS hybrid design is much better than that of the SA hybrid design for any number of BS antennas and iterations. The proposed DCIFS hybrid design with $K = 1$ outperforms the SA hybrid design with $K = 10$ which means that our design with a very low number of iterations K performs better than the SA design, resulting in a reduced computational complexity.

In Fig 11, we use the same parameters as in Fig. 5, but we increase the number of data streams to 4. As we see in Fig 11, similar to the previous figure, because we use the SA architecture in BS and MS, the performance of the proposed DCIFS and SA hybrid design is degraded compared to the results in Fig. 6. The gain of the proposed DCIFS hybrid design over the SA hybrid design is very high for any number of BS antennas and iterations. Also, the proposed DCIFS hybrid design with $K = 1$ outperforms the SA hybrid design with $K = 10$, which shows the advantage of our design compared to the SA hybrid
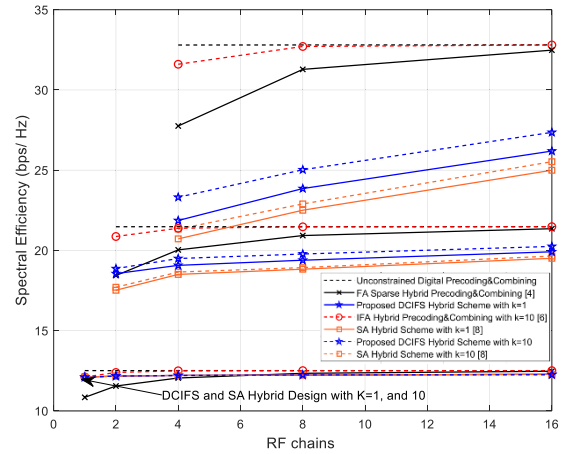

FIGURE 9. Average spectral efficiency achieved by the proposed DCIFS hybrid precoders/combiners with different *K* compared to the FA sparse hybrid precoders/combiners [4], the optimal unconstrained digital precoders/combiners, IFA hybrid precoders/combiners [6] with *K* = 10, and the SA hybrid precoders/combiners with different *K* in 144 × 64 UPAs mmWave systems for SNR = 0 dB with $N_S \in \{1, 2, 4\}$ and different RF chains.
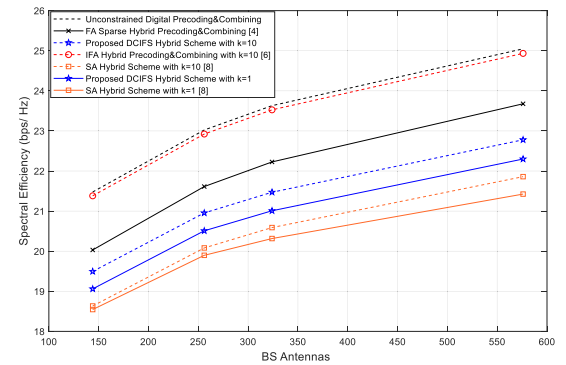

FIGURE 10. Average spectral efficiency vs the number of BS antenna achieved by the proposed DCIFS hybrid precoders/combiners with different *K* compared to the FA sparse hybrid precoders/combiners [4], the optimal unconstrained digital precoders/combiners, IFA hybrid precoders/combiners [6] with *K* = 10, and the SA hybrid precoders/combiners [8] with different *K* in UPAs mmWave systems for SNR = 0 dB with $N_r = 64$, $N_S = 2$ and $N_{tRF} = N_{rRF} = 4$.

FIGURE 11. Average spectral efficiency vs the number of BS antenna achieved by the proposed DCIFS hybrid precoders/combiners with different *K* compared to the full array sparse hybrid precoders/combiners [4], the optimal unconstrained digital precoders/combiners, IFA hybrid precoders/combiners [6] with *K* = 10, and the SA hybrid precoders/combiners [8] with different *K* in UPAs mmWave systems for SNR = 0 dB with $N_r = 64$, $N_S = 4$ and $N_{tRF} = N_{rRF} = 4$.
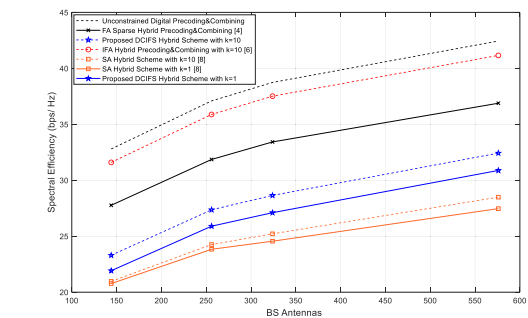
design because we take into consideration the matrix structure of the analog and baseband precoding and combining in the DCIFS hybrid design derivation.

In conclusion, although we use the proposed DCIFS hybrid design in both transmitter and receiver, its performance is acceptable compared to the higher hardware complexity FA designs such as the sparse hybrid design and the IFA hybrid design. All full array hybrid designs require higher hardware complexity in the BS and MS, higher number of phase shifters in the BS and MS. The performance of the proposed DCIFS hybrid design with a small number of iterations is considerably better compared to the SA hybrid design, especially for a large number of BS antennas. Taking advantage of the structure of the analog and baseband precoding/combing matrices in the proposed DCIFS hybrid design is the key point to achieve high performance and outperform the SA hybrid design. The number of iterations should be 10 or less because after that the gain will be very small which is confirmed by results that we did not include in this paper.

VI. CONCLUSION

In this paper, we have proposed a new approach called DCIFS to design hybrid precoding and combining for mmWave MIMO systems with SA architecture. The proposed design algorithm involves an iterative process that begins by designing a hybrid precoding and combining matrix for the FA structure and then converts it into an SA matrix by setting certain entries to zero while maintaining FA performance. We have studied two scenarios with the suggested algorithm and compared them with other existing FA and SA hybrid precoding and combining designs. In the first scenario, we employed the proposed DCIFS hybrid precoding at the BS and the iterative FA hybrid combining at the MS, while in the second scenario, we employed the proposed DCIFS hybrid design at both the BS and the MS. The simulation results demonstrated that the proposed DCIFS algorithm achieves spectral efficiency that is comparable to that of the FA design and outperforms the conventional SA hybrid design with a small number of iterations, especially for large systems. The results also showed that the number of iterations suitable for the proposed hybrid design should be 10 or less. The hardware complexity of the proposed DCIFS hybrid design is the same as that of the conventional SA hybrid design and lower than that of the FA hybrid design, indicating that the proposed DCIFS design is a suitable solution for future communication systems. For future work, it would be interesting to extend this work to a multi-user scenario. This would allow for a more comprehensive evaluation of the proposed approach and enable its potential application in practical scenarios where multiple users are present.

REFERENCES

[1] Z. Pi and F. Khan, "An introduction to millimeter-wave mobile broadband systems," *IEEE Commun. Mag.*, vol. 49, no. 6, pp. 101–107, Jun. 2011.
[2] T. S. Rappaport, "Millimeter wave mobile communications for 5G cellular: It will work!" *IEEE Access*, vol. 1, pp. 335–349, 2013.
[3] M. Xiao, "Millimeter wave communications for future mobile networks," *IEEE J. Sel. Areas Commun.*, vol. 35, no. 9, pp. 1909–1935, Sep. 2017.
[4] O. E. Ayach, S. Rajagopal, S. Abu-Surra, Z. Pi, and R. Heath Jr., "Spatially sparse precoding in millimeter wave MIMO systems," *IEEE Trans. Wireless Commun.*, vol. 13, no. 3, pp. 1499–1513, Mar. 2014.

[5] A. Alkhateeb, J. Mo, N. Gonzalez-Prelcic, and R. W. Heath Jr., "MIMO precoding and combining solutions for millimeter-wave systems," *IEEE Commun. Mag.*, vol. 52, no. 12, pp. 122–131, Dec. 2014.
[6] M. Alouzi, F. Chan, and C. D'Amours, "Low complexity hybrid precoding and combining for millimeter wave systems," *IEEE Access*, vol. 9, pp. 95911–95924, 2021.
[7] S. Park, A. Alkhateeb, and R. W. Heath Jr., "Dynamic subarrays for hybrid precoding in wideband mmWave MIMO systems," *IEEE Trans. Wireless Commun.*, vol. 16, no. 5, pp. 2907–2920, May 2017.
[8] F. Al-Kamali and C. D'amours, "Low-complexity hybrid precoding for subarray architecture mmWave MIMO systems," *IEEE Access*, vol. 10, pp. 74921–74930, 2022.
[9] R. Mendez-Rial, C. Rusu, N. Gonzalez-Prelcic, and R. W. Heath Jr., "Dictionary-free hybrid precoders and combiners for mmWave MIMO systems," in *Proc. IEEE 16th Int. Workshop Signal Process. Adv. Wireless Commun. (SPAWC)*, Jun. 2015, pp. 151–155.
[10] C.-E. Chen, "An iterative hybrid transceiver design algorithm for millimeter wave MIMO systems," *IEEE Wireless Commun. Lett.*, vol. 4, no. 3, pp. 285–288, Jun. 2015.
[11] L. Liang, W. Xu, and X. Dong, "Low-complexity hybrid precoding in massive multiuser MIMO systems," *IEEE Wireless Commun. Lett.*, vol. 3, no. 6, pp. 653–656, Dec. 2014.
[12] F. Dong, W. Wang, and Z. Wei, "Low-complexity hybrid precoding for multi-user mmWave systems with low-resolution phase shifters," *IEEE Trans. Veh. Technol.*, vol. 68, no. 10, pp. 9774–9784, Oct. 2019.
[13] J. Du, W. Xu, H. Shen, X. Dong, and C. Zhao, "Hybrid precoding architecture for massive multiuser MIMO with dissipation: Sub-connected or fully connected structures?" *IEEE Trans. Wireless Commun.*, vol. 17, no. 8, pp. 5465–5479, Aug. 2018.
[14] H. Li, M. Li, Q. Liu, and A. L. Swindlehurst, "Dynamic hybrid beamforming with low-resolution PSs for wideband mmWave MIMO-OFDM systems," *IEEE J. Sel. Areas Commun.*, vol. 38, no. 9, pp. 2168–2181, Sep. 2020.
[15] Y. Liu and J. Wang, "Low-complexity OFDM-based hybrid precoding for multiuser massive MIMO systems," *IEEE Wireless Commun. Lett.*, vol. 9, no. 3, pp. 263–266, Mar. 2020.
[16] X. Gao, L. Dai, S. Han, I. Chih-Lin, and R. W. Heath, "Energy-efficient hybrid analog and digital precoding for mmWave MIMO systems with large antenna arrays," *IEEE J. Sel. Areas Commun.*, vol. 34, no. 4, pp. 998–1009, Apr. 2016.
[17] S. He, C. Qi, Y. Wu, and Y. Huang, "Energy-efficient transceiver design for hybrid sub-array architecture MIMO systems," *IEEE Access*, vol. 4, pp. 9895–9905, 2016.
[18] N. Li, Z. Wei, H. Yang, X. Zhang, and D. Yang, "Hybrid precoding for mmWave massive MIMO systems with partially connected structure," *IEEE Access*, vol. 5, pp. 15142–15151, 2017.
[19] W. Huang, Z. Lu, Y. Huang, and L. Yang, "Hybrid precoding for single carrier wideband multi-subarray millimeter wave systems," *IEEE Wireless Commun. Lett.*, vol. 8, no. 2, pp. 484–487, Apr. 2019.
[20] P. Zhao and Z. Wang, "Hybrid precoding for millimeter wave communications with fully connected subarrays," *IEEE Commun. Lett.*, vol. 22, no. 10, pp. 2160–2163, Oct. 2018.
[21] J. Deng, O. Tirkkonen, and C. Studer, "MmWave multiuser MIMO precoding with fixed subarrays and quantized phase shifters," *IEEE Trans. Veh. Technol.*, vol. 68, no. 11, pp. 11132–11145, Nov. 2019.
[22] F. Al-Kamali, C. D'Amours, and F. Chan, "Hybrid precoding for mmWave MIMO systems with overlapped subarray architecture," *IEEE Access*, vol. 10, pp. 130699–130707, 2022.
[23] L. Yan, C. Han, and J. Yuan, "A dynamic array of sub-array architecture for hybrid precoding in the millimeter wave and terahertz bands," in *Proc. IEEE Int. Conf. Commun. Workshops (ICC Workshops)*, May 2019, pp. 1–5.
[24] X. Wang, J. Wang, and X. Shi, "A low-complexity hybrid precoding scheme for mmWave MIMO systems with dynamic subarrays," in *Proc. IEEE Int. Symp. Broadband Multimedia Syst. Broadcast. (BMSB)*, Chengdu, China, Aug. 2021, pp. 1–5.
[25] R. Magueta, D. Castanheira, A. Silva, R. Dinis, and A. Gameiro, "Hybrid multi-user equalizer for massive MIMO millimeter-wave dynamic subconnected architecture," *IEEE Access*, vol. 7, pp. 79017–79029, 2019.
[26] S. Park, A. Alkhateeb, and R. W. Heath Jr., "Dynamic subarray architecture for wideband hybrid precoding in millimeter wave massive MIMO systems," in *Proc. IEEE Global Conf. Signal Inf. Process. (GlobalSIP)*, Washington, DC, USA, Dec. 2016, pp. 600–604.

[27] J. Jiang, Y. Yuan, and L. Zhen, "Multi-user hybrid precoding for dynamic subarrays in mmWave massive MIMO systems," *IEEE Access*, vol. 7, pp. 101718–101728, 2019.

[28] F. Yang, J.-B. Wang, M. Cheng, J.-Y. Wang, M. Lin, and J. Cheng, "A partially dynamic subarrays structure for wideband mmWave MIMO systems," *IEEE Trans. Commun.*, vol. 68, no. 12, pp. 7578–7592, Dec. 2020.

[29] K. B. Dsouza, K. N. R. S. V. Prasad, and V. K. Bhargava, "Hybrid precoding with partially connected structure for millimeter wave massive MIMO OFDM: A parallel framework and feasibility analysis," *IEEE Trans. Wireless Commun.*, vol. 17, no. 12, pp. 8108–8122, Dec. 2018.

[30] X. Song, T. Kuhne, and G. Caire, "Fully-/partially-connected hybrid beamforming architectures for mmWave MU-MIMO," *IEEE Trans. Wireless Commun.*, vol. 19, no. 3, pp. 1754–1769, Mar. 2020.

[31] C.-C. Hu and J.-H. Zhang, "Hybrid precoding design for adaptive subconnected structures in millimeter-wave MIMO systems," *IEEE Syst. J.*, vol. 13, no. 1, pp. 137–146, Mar. 2019.

[32] C.-C. Hu and C.-W. Hsu, "Efficient adaptive subarrays in millimeter-wave MIMO systems with hybrid RF/baseband precoding/combining design," *IEEE Syst. J.*, vol. 13, no. 4, pp. 3735–3746, Dec. 2019.

[33] Z. Zhang, X. Wu, and D. Liu, "Joint precoding and combining design for hybrid beamforming systems with subconnected structure," *IEEE Syst. J.*, vol. 14, no. 1, pp. 184–195, Mar. 2020.

[34] A. M. Elbir and A. K. Papazafeiropoulos, "Hybrid precoding for multiuser millimeter wave massive MIMO systems: A deep learning approach," *IEEE Trans. Veh. Technol.*, vol. 69, no. 1, pp. 552–563, Jan. 2020.

[35] K. M. Attiah, F. Sohrabi, and W. Yu, "Deep learning for channel sensing and hybrid precoding in TDD massive MIMO OFDM systems," *IEEE Trans. Wireless Commun.*, vol. 21, no. 12, pp. 10839–10853, Dec. 2022.

[36] H. Hojatian, J. Nadal, J.-F. Frigon, and F. Leduc-Primeau, "Flexible unsupervised learning for massive MIMO subarray hybrid beamforming," in *Proc. IEEE Global Commun. Conf. (GLOBECOM)*, Rio de Janeiro, Brazil, Dec. 2022, pp. 3833–3838.

[37] Q. Yuan, H. Liu, M. Xu, Y. Wu, L. Xiao, and T. Jiang, "Deep learning-based hybrid precoding for terahertz massive MIMO communication with beam squint," *IEEE Commun. Lett.*, vol. 27, no. 1, pp. 175–179, Jan. 2023.

[38] P. H. Schönemann, "A generalized solution of the orthogonal Procrustes problem," *Psychometrika*, vol. 31, no. 1, pp. 1–10, Mar. 1966.

[39] C. Rusu, R. Mendez-Rial, N. Gonzalez-Prelcic, and R. W. Heath Jr., "Low complexity hybrid precoding strategies for millimeter wave communication systems," *IEEE Trans. Wireless Commun.*, vol. 15, no. 12, pp. 8380–8393, Dec. 2016.

FAISAL AL-KAMALI received the B.Sc. degree in electronics and communication engineering from the University of Baghdad, Baghdad, Iraq, in 2001, and the M.Sc. and Ph.D. degrees in communication engineering from the University of Minufia, Egypt, in 2008 and 2011, respectively. He joined the Electrical Engineering Department, University of Ibb, Ibb, Yemen, in 2011, as an Assistant Professor and became an Associate Professor, in January 2017. He was the Head of the Electrical Engineering Department, Faculty of Engineering, University of Ibb, from 2013 to 2014, where he was the Vice Dean of Academic Affairs with the Faculty of Engineering, from 2018 to 2020. Since November 2021, he has been a Visiting Scholar with the Faculty of Engineering, School of Electrical Engineering and Computer Science, University of Ottawa, Canada. His research interests include physical layer technologies for wireless communication systems, such as interference cancellation, channel equalization and channel estimation, image transmission over wireless communication systems, hybrid precoding and combining, mmWave systems, and massive MIMO systems. He was a recipient of the prize for supervising the best graduation project with Ibb University, in 2016.

CLAUDE D'AMOURS (Member, IEEE) received the B.A.Sc., M.A.Sc., and Ph.D. degrees in electrical engineering from the University of Ottawa, in 1990, 1992, and 1995, respectively. He was a Systems Engineer with Calian Communications Systems Ltd., and Communications Research Centre, Ottawa, in 1992 and 1995, respectively. Later in 1995, he joined the Department of Electrical and Computer Engineering, Royal Military College, Canada, as an Assistant Professor. He joined the School of Electrical Engineering and Computer Science, University of Ottawa, in 1999, where he was the Vice Dean of Undergraduate Studies with the Faculty of Engineering, from 2007 to 2011, and the Director of the School of Electrical Engineering and Computer Science, from 2013 to 2022. He is currently the Interim Vice Dean of Graduate Studies with the Faculty of Engineering, University of Ottawa. His research interests include physical layer technologies for wireless and optical communication systems, such as multiple access, interference cancellation, modulation, coding, and signal processing.

MOHAMED ALOUZI (Student Member, IEEE) received the B.S. degree in electrical and computer engineering from Zawiya University, Al-Zāwiyah, Libya, in 2009, the M.A.Sc. degree in electrical engineering from the Royal Military College of Canada, Kingston, Canada, in 2017, and the Ph.D. degree in electrical engineering from the University of Ottawa, Ottawa, Canada, in 2023. His research interests include millimeter waves, 5G and beyond systems, and hybrid beamforming.

FRANCOIS CHAN (Senior Member, IEEE) received the B.Eng. degree in electrical engineering from McGill University, Montreal, Canada, and the M.Sc.A. and Ph.D. degrees in electrical engineering from Ecole Polytechnique de Montréal, Canada. He was a Visiting Researcher with the University of California at Irvine, Irvine, in 2002 and 2005. He is currently a Professor with the Department of Electrical and Computer Engineering, Royal Military College of Canada, Kingston, ON, Canada. He is also an Adjunct Professor and a Visiting Professor with the University of Ottawa. His research interests include digital communications, wireless communications, and digital signal processing.

● ● ●